Detection of improper mounting from the sensor signal of vortex flowmeters

A. G. Rossberg[+], P. Riegler[*], F. Buhl[×], J. Herwig[×], and J. Timmer[+]

[+]Center for Data Analysis and Modeling (FDM), University of Freiburg, Germany
[*]University of Applied Sciences Braunschweig/Wolfenbüttel, Germany
[×]ABB Automation Products GmbH, Göttingen, Germany

May 2003

Abstract

In vortex flowmeters, the frequency of vortex formation at a bluff body inserted into the flow is used to determine the flow velocity. The frequency is determined using a sensor that measures the time-dependent distortions of the down-stream flow field. But the (univariate) sensor signal contains more information than just the vortex frequency. We use this inherent extra information to verify if the pipe flow has the form expected for the correct mounting of the flowmeter, and thus, if the flow measurement has the expected high accuracy. In designing the method, special care was taken to leave it robust with respect to uncertainties in the material properties of the fluid. In order to achieve this goal, the method makes use of the scaling properties of the Navier-Stokes equation. We present the theoretical background of the proposed diagnostic functionality and verify it on measurement data. In the experiments, irregularities that lead to more than 0.5% error in the output of the flowmeter can clearly be detected.

1 Introduction

Vortex flowmeters are widely use in industrial flow metering, for example in chemical industries, pulp and paper industries, power plants, and for all kinds of gas measurements. Particular advantages of this technology are the low cost of maintenance for the devices, their robustness to extreme condition, and their comparatively high accuracy. The measurement principle of vortex flowmeters makes use of the von-Karman vortex street which forms downstream behind a long, thin, solid body, the *vortex shedder* or *bluff body*, extended normal to the flow. The frequency of vortex formation is a function of the flow velocity. To a good approximation, the functional relation is linear. Thus, by measuring the frequency, the flow velocity or, for pipe flow, the volume flow rate can be

determined. To detect the vortex oscillations behind the bluff body, two types of sensors are generally used. Ultrasound barriers (e.g., [1]) and sensors measuring "pressure", i.e. reactive surface forces at the pipe boundaries, on "paddles" inserted into the flow, or at the bluff body itself. The second type often makes use of the piezoelectric effect.

It is well known, that "the calibrations of flowmeters are dependent to some extent on the geometry of the pipework and fittings both upstream and downstream" [2]. Deviations from the specifications given by the manufacturer can bias the measured flow rate. Similar effects result from deposits at or erosion of the bluff body or the pipe. This problem is not specific to vortex flowmeters [3]. If this susceptibility to faulty conditions cannot be avoided, it is desirable that the flowmeter does at least detect such faulty conditions, such that the user can be alerted by a warning message issued automatically by the flowmeter. This can be done by a simple warning light, or by a message on the field bus, which could then also contain information regarding the severity of the fault and an error estimate, a concept known as self-validating sensor (SEVA) [4].

Various schemes to detect faulty conditions have been proposed. It is common to these methods that some quantitative characterizations of the signal are computed and compared with the values for normal conditions. Deviations are identified as faults. The characterizations used have been based on the second order statistics (power spectra or correlation functions) of the sensor signal [5, 6], or on the statistical analysis of intermediate results of the signal processing for the flow rate [7, 8, 9].

The method proposed here is based on a signal model which takes the nonlinear nature of the vortex dynamics explicitly into account. We argue that the characterizations derived on the basis of this signal model make use of essentially all information available. But there is another point that has to be addressed. Even for the unperturbed flow with correctly mounted flow meter, the sensor signal depends on the flow rate and on various material properties of the fluid. It seems that, in order to be able to detect deviant conditions, characterizations of the signal for a large number or "normal" conditions have to be recorded at the flowmeter, and the correct one has to be selected at each instant. The feasibility of this approach is therefore not immediately clear.

Here we show that, by making use of the scaling properties of the Navier-Stokes equation, appropriate characterizations of the signal can be constructed which depend only weakly on the material parameters or the flow rate, and are sensitive to faulty mounting. In Section 2 the theoretical background for selecting appropriate characterizations is laid out. Based on these results, specific characterizations are defined in Section 3. These are applied to experimental data in Section 4. Section 5 summarizes the results.

2 Modeling the sensor signal

2.1 Basic theory

The pipe flow through the vortex flowmeter is described by the Navier-Stokes equation for incompressible media

$$\dot{\mathbf{v}} + (\mathbf{v} \cdot \nabla)\mathbf{v} = -\rho^{-1}\nabla p + \nu\nabla^2\mathbf{v}, \tag{1}$$

with the velocity $\mathbf{v} = \mathbf{v}(\mathbf{r}, t)$, the pressure $p = p(\mathbf{r}, t)$, the mass density ρ, and the kinematic viscosity ν, supplemented with the incompressibility condition

$$\nabla \cdot \mathbf{v} = 0 \tag{2}$$

and appropriate boundary conditions. With typical length scales L of the order of the pipe diameter d [10] and typical velocities of the order Q/d^2, where Q is the volume flow rate, typical time scales are of the order $T := d^3/Q$. Hence, the two terms on the left hand side (l.h.s.) of (1) are both of the order $L/T^2 = Q^2/d^5$. The viscous term on the right hand side (r.h.s.) is to a first approximation of the order $1/(L\,T) = \nu Q/d^4$. It is thus by a factor of the size of the Reynolds number $Re := 4\,Q/(\pi\,d\,\nu)$ smaller than the l.h.s.. In order for (2) to be satisfied, the pressure term on the r.h.s. of the Navier-Stokes equation (1) has to balance the dominating terms on the l.h.s. for large Re. It is therefore also of the order Q^2/d^5.

It is now important to notice that neither the phenomenon of vortex shedding nor the short-term dynamics of the resulting von-Karman vortex street do essentially depend on viscous effects (vortex shedding has been observed even in Bose-Einstein condensates, inviscid "quantum fluids" [11, 12]). At high Reynolds numbers, viscous effects enter merely as small corrections, roughly of the order Re^{-1}. Of course, due to turbulence, the effective viscosity is larger than ν, and the decay of viscous effects is not quite as fast as Re^{-1}. Thin, viscously dominated boundary layers do also remain. But the overall effect persists. The higher the Reynolds number, the better the bulk vortex dynamics at not too large distance from the bluff body are described by the inviscid ($\nu \to 0$) limit. On the other hand, for small Re, viscous effects suppress vortex shedding.

A straightforward analysis shows that in the limit $\nu \to 0$ solutions of (1,2) are, up to scaling, independent of Q, with velocities $\sim Q$ and times $\sim Q^{-1}$. (We assume the flowmeter's geometry to be fixed, hence the length scale is fixed.) This is why the proportionality of the frequency of vortex shedding f and the flow rate Q is satisfied so well that, in simple vortex flowmeters, $f \times K^{-1}$, with an appropriate "K-factor" K, is used as a direct measure of Q without corrections. In modern vortex flowmeters, corrections to the scaling law are taken into account, e.g., by using a Re-dependent K. Since the Re-dependence of K is weak, it is easily determined and stored in the flowmeter based on measurements of a few data points only. Below we will make use of this approximate scaling law also for other characterizations of the flow pattern.

2.2 The signal model

It is well known [13, 14, 15, 16, 17, 18], that the signal $x(t)$ of a sensor mounted behind a vortex shedder in a laminar flow can be described by the Stuart-Landau Equation

$$\dot{A} = (\epsilon + i\omega_0)A - (g_r + i\, g_i)|A|^2 A, \tag{3}$$

where $A = A(t)$ is the complex amplitude of the signal, $x(t) = A(t) + (\beta_r + i\,\beta_i)A^2(t) + (\gamma_r + i\,\gamma_i)A^3(t) + c.c. + [\text{higher order terms}]$, and ϵ, ω_0, g_r, g_i, β_r, β_i, γ_r, γ_i are real parameters to be chosen appropriately with $\omega_0, g_r > 0$. With a symmetric setup of flow, bluff body, and sensor, $\beta_r = \beta_i = 0$.

Under the conditions where vortex flowmeters are used, the inlet flow is usually not laminar ($Re \approx 10^4 - 10^5$). The effect of turbulence can be modeled by supplementing Eq. (3) with a noise term, i.e.

$$\dot{A} = (\epsilon + i\omega_0)A - (g_r + i\, g_i)|A|^2 A + \zeta, \tag{4}$$

where

$$\langle \zeta(t)\zeta(t') \rangle = 0, \text{ and } \langle \zeta(t)\zeta^*(t') \rangle = 4F\delta(t - t'), \tag{5}$$

with $\langle \cdot \rangle$ denoting the expectation value.

In order to take also the small-scale turbulence near the sensor into account, the signal must now be expressed as

$$x(t) = A(t)+(\beta_r+i\,\beta_i)A^2(t)+(\gamma_r+i\,\gamma_i)A^3(t)+c.c.+[\text{noise}]+[\text{higher order terms}]. \tag{6}$$

In principle, bifurcation theory leads to these results by the mere fact that the onset of vortex formation is a supercritical (= forward, continuous) Hopf bifurcation (= transition to oscillation from a steady state), either with [19] or without noise [20]. However, in other systems that satisfy these conditions, the range of validity of the Stuart-Landau Equation is limited to a small range in control parameter space near the bifurcation point (i.e., the point corresponding to $\epsilon = 0$).

An analysis of experimental time series reveals that for von-Karman vortices in vortex flowmeters the range of validity of Eqs. (4,5) extends over the complete working range of the flowmeter, at least in a semi-quantitative sense. This can be understood by the results of Sec. 2.1. Three ranges for the Reynolds number have to be distinguished: (i) At low Reynolds numbers, vortex shedding is suppressed by viscous damping. (ii) In the cross-over region vortex shedding sets in. (iii) At higher Reynolds numbers the large-scale flow pattern is independent of *Re* up to scaling. Apparently, the cross over region (ii) is narrow, and the transition from (ii) to (iii) is still close enough to the bifurcation point such that Eqs. (4,5) hold. By the scaling behaviors of the solution, Eqs. (4,5) are than valid over the complete range (iii). Hence, those characterizations of the sensor-signal will be particularly useful which are sensitive to changes in the parameters in Eqs. (4-6).

2.3 Dependence of the signal on material parameters

Regarding the dependency of the sensor signal on the material parameters of the fluid in the pipe, two aspects have to be distinguished: (a) dependencies due to the particular sensor technology at given flow field and (b) dependencies by the dependencies of the flow field itself on material parameters. As far as (a) is concerned, we shall here assume that only the amplitude of the sensor signal depends on material parameters, i.e., the sensor signal is independent of the material up to a constant factor. For example, for sensors sensitive to reactive forces exerted by the fluid on the solid boundary (e.g., a paddle reaching into the fluid), the signal is, at fixed flow rate, proportional to the mass density of the fluid. For ultrasonic sensors, the phase modulation of the recorded wave train, for example, is inversely proportional to the square of the velocity of sound in the fluid.

In order to understand the dependence (b) of the signal on material parameters through the flow field, the well known scaling laws for the Navier-Stokes equation (1) can be used. The flow field at fixed volume flow depends on the material only through the kinematic viscosity. If $\mathbf{v}(\mathbf{r},t) = \mathbf{v}_0(\mathbf{r},t)$ (and a corresponding $p(\mathbf{r},t)$) is a solution of (1,2) with viscosity $\nu = \nu_0$, then $\mathbf{v}(\mathbf{r},t) = \mathbf{v}_0'(\mathbf{r},t) = s\mathbf{v}_0(\mathbf{r},s\,t)$ is a solution of (1,2) at viscosity $\nu = s\,\nu_0$ for any positive s. Obviously, the flow rate Q for $\mathbf{v}_0'$ is s times larger than the flow rate for $\mathbf{v}_0$ and the solutions $\mathbf{v}_0$ and $\mathbf{v}_0'$ have to the same Reynolds number. Corresponding relations hold also for the probability distribution of the random velocity field in turbulent flow. Now, assume that, for a given viscosity ν_0, the (random) flow field $\mathbf{v}_0(\mathbf{r},t)$ is known for all flow rates Q. Then the flow field for viscosity $\nu_0' = s\,\nu_0$ at flow rate Q' is $\mathbf{v}(\mathbf{r},t) = \mathbf{v}_0'(\mathbf{r},t) = s\,\mathbf{v}_0(\mathbf{r},s\,t)$, where $\mathbf{v}_0(\mathbf{r},t)$ is the flow field for viscosity ν_0 at flow rate $Q = s^{-1}\,Q'$. When the dependence of the flow field on the flow rate is known for one viscosity, it is known for all viscosities.

It is desirable to preserve this scaling behavior for the sensor signal $x(t)$. The scaling behavior is preserved if $x(t)$ depends on $\mathbf{v}(\mathbf{r},t)$ in such a way that, when $\mathbf{v}(\mathbf{r},t) = \mathbf{v}_0(\mathbf{r},t)$ leads to the signal $x(t) = x_0(t)$, then $\mathbf{v}(\mathbf{r},t) = s\,\mathbf{v}_0(\mathbf{r},s\,t)$ leads to $x(t) = f(s)\,x_0(s\,t)$. The function $f(s)$ is typically a power of s. Since the overall amplitude of $x(t)$ depends on the material parameters of the particular fluid anyway, the precise form of $f(s)$ is not relevant here. Both reactive-force and ultrasound flow sensing lead to signals which are linear functionals in the instantaneous flow field [i.e., they do not depend on time derivatives of $\mathbf{v}(\mathbf{r},t)$], and the scaling law for the signal is satisfied with both technologies.

3 Characteristic quantities

The strategy to detect improper mounting of the flowmeter is to obtain several quantitative characterizations, *features*, of the sensor signal and to verify if these features are in the range expected for proper mounting. Ideally, these features depend as little as possible on the flow rate and the material parameters of the

fluid, and are sensitive to the geometry of the flow. Features that give the same value for the two signals $x(t) = x_0(t)$ and $x(t) = u\,x_0(s\,t)$ with any positive u and s are particularly well suited for this task: By the discussion in Sec. 2.3, such features depend, with proper mounting, only on the Reynolds number. By the results of Sec. 2.1, the flow field, and thus the signal, vary, up to scaling, only little with the Reynolds number. Since the features are assumed to be invariant under scaling, it follows that their dependence on the Reynolds number is weak.

The higher the number of independent features that can be used to classify the flow, the more reliable is the diagnosis. In order to estimate the number of independent features that can be extracted from the signal, we make use of the model (4-6). It has the nine free parameters ϵ, ω_0, g_r, g_i, F, β_r, β_i, γ_r, γ_i. Two degrees of freedom depend on material properties and should not be used as characterizations. Thus, as far as our model of the signal is good [21], there are at most seven independent features.

One of these features is the angular oscillation frequency $\omega = 2\,\pi\,f$, which is used to determine the flow rate. It is determined from the signal using standard methods. The period $2\pi/\omega$ is used as a natural time scale, which can be used to make the features invariant with respect to scaling of time. For the model (4) ω is, with not too strong noise, roughly given by $\omega \approx \omega_0 - g_i\epsilon/g_r$.

For the subsequent analysis, the fundamental mode of oscillation is extracted from the signal. This is achieved by convoluting the signal with the Morlet wavelet

$$w(t) = \frac{\Delta\omega}{\sqrt{2\pi}} \exp\left(i\,\omega\,t - \frac{1}{2}(\Delta\omega\,t)^2\right), \tag{7}$$

where the band width $\Delta\omega = 0.2\,\omega$ was chosen such as to optimize the sensitivity of the characterizations. The result of the convolution, $z(t) = w(t) * x(t)$ is an estimate for the complex signal amplitude $A(t)$ of Eq. (4). It can also be interpreted as the analytic signal corresponding to $x(t)$ after band-pass filtering. The filtering also eliminates most of the measurement noise.

From $z(t)$ the instantaneous frequency [22]

$$\omega_i(t) = \mathrm{Im}\left\{\frac{\dot{z}(t)}{z(t)}\right\} \tag{8}$$

and the phase

$$\phi(t) = \int_0^t \omega_i(t')dt' \tag{9}$$

are obtained. As a measure for the phase stability of the oscillation, the feature D given by

$$D := \frac{\mathrm{var}[\phi(t + 2\pi\,n/\omega) - \phi(t)]}{n} \tag{10}$$

with $n = 10$ is used. As is easily verified, D satisfies the scaling invariance as required. Using the model (4-6), one obtains $D \approx 4\pi\,F\,(g_r + g_i^2/g_r)/\epsilon\,\omega$ in the weak noise limit [23]. The feature

$$S := \frac{\left\langle |z(t)|^2 \right\rangle - \left\langle |z(t)| \right\rangle^2}{\left\langle |z(t)| \right\rangle^2}, \tag{11}$$

is a measure for the strength of fluctuations in the signal amplitude. It is estimated as $S \approx F g_r/4\epsilon^2$.

A feature quantifying the nonlinear frequency shift is, for example, given by

$$R := \frac{\left\langle |z(t)|^2 \omega_i(t) \right\rangle - \left\langle |z(t)|^2 \right\rangle \langle \omega_i(t) \rangle}{\langle |z(t)|^2 \rangle \langle \omega_i(t) \rangle}. \tag{12}$$

Approximately, one has $R \approx -2\,F\,g_i/\epsilon\,\omega$.

Finally, amplitude and phase of higher harmonics can be used to characterize the signal. This leads to the features

$$B = B_r + iB_i := \frac{\left\langle \overline{z}(t)^2 x(t) \right\rangle}{\langle |z(t)| \rangle^3} \tag{13}$$

and

$$G = G_r + iG_i := \frac{\left\langle \overline{z}(t)^3 x(t) \right\rangle}{\langle |z(t)| \rangle^4}, \tag{14}$$

where the overline denotes complex conjugation. For model (4-6), $B \approx (\beta_r + i\beta_i)(\epsilon/g_r)^{1/2}$ and $G \approx (\gamma_r + i\gamma_i)(\epsilon/g_r)$, respectively. Obviously, S, R, B, and G do also satisfy the desired scaling invariance. Using the approximation formulas given above, it is also readily verified that the seven features that have been introduced span, up to scaling of time and amplitude, the full parameter space of the model (4-6). Introduction of further features would therefore not lead to significantly better characterizations.

4 Experimental results

4.1 Experimental setup

Measurements were performed on a vortex flowmeter VORTEX VT4000 DN150-ANSI [24], with water at 20° C streaming steadily out of a large tank. Apart from the irregularities imposed for the experimental purpose, the mounting conditions conformed to the specifications of the device. The flow was measured independently using an inductive flowmeter mounted upstream. The flow rate and the oscillatory signal of the vortex sensor (frequencies in the rage 2-13 Hz) were recorded at a sampling rate of at least 1 kHz using a digital data recorder (Viper-TA, Gould). Data analysis was performed offline using the MATLAB software package.

4.2 The reference experiment

In order to verify the prediction that the features introduced above do in fact depend only little on Re, and to obtain reference data for a test for inappropriate mounting, the dependence of the features D, S, and G on the flow rate was determined. The setup used was always symmetric, so $B \equiv 0$. The feature R

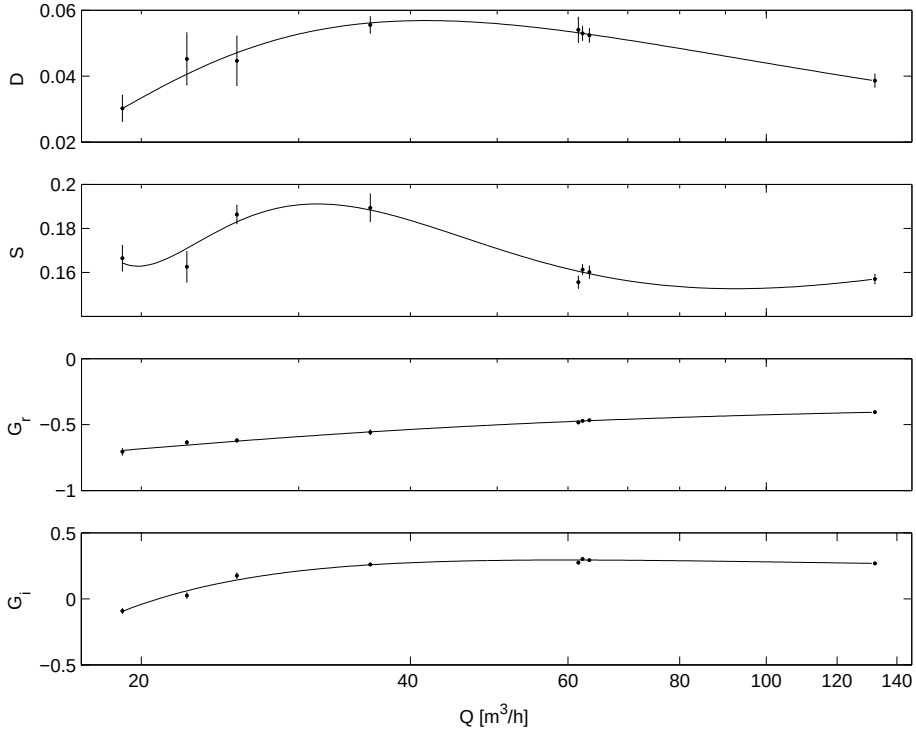

Figure 1: The dependence of the features D, S, and $G = G_r + iG_i$, defined in Section 3 for a correctly mounted flowmeter. The points correspond to measurements (1-σ errorbars), the curves to polynomial fits.

turned out to be too sensitive to external perturbations. It is therefore not used for the analysis.

The features were measured using time series of one minute duration at flow rates Q = 19-132 m^3/h, with the expectation values $\langle\cdot\rangle$ estimated by temporal averages. Measurements were repeated 8-43 times at each flow rate, and the average values of the features and their covariance matrix were calculated. The functional dependence of the features and the covariance matrix on the flow rate Q was then estimated using polynomial interpolation of the data. Leave-one-out cross validation was used to guard against overfitting. Third, fourth, and second order polynomials were used to fit D, S, and G, respectively. The full covariance matrix was taken into account to optimize the fit. For the covariance matrix itself a linear fit was used. Figure 1 shows the measured and fitted reference data. As expected, the dependence on Q, respectively Re, is weak, especially for high Q ($Q > 60\,\mathrm{m}^3/\mathrm{h}$).

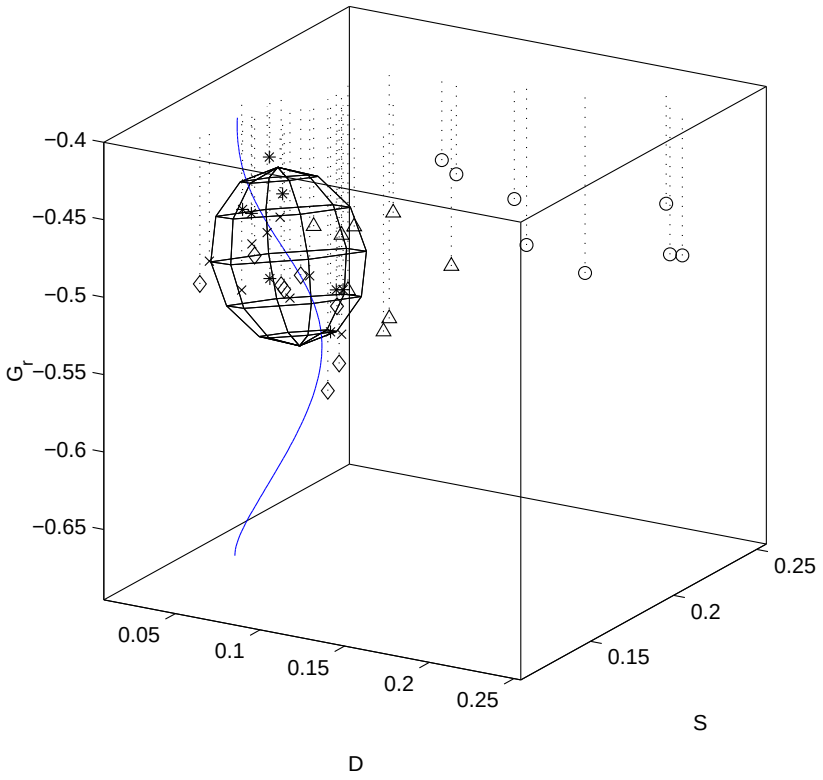

Figure 2: A 3D view of the measured features D, S, and G_r for inappropriate mounting, see Section 4.3. Data points are drawn as "hanging down" from the upper face of the enclosing box. Stars: correct mounting; ×: DIN/ANSI mismatch; diamonds, triangles, and circles: off-axis mounting with 5 mm, 10 mm, and 15 mm eccentricity. The solid curve corresponds to the expectation values for correct mounting, parameterized by the flow rate Q. The ellipsoid is the 95% confidence interval for correct mounting at $Q = 50\,\mathrm{m}^3/\mathrm{h}$ (assuming Gaussian errors).

4.3 Detection of improper mounting

Data was collected with flowmeters mounted improperly in order to investigate if this could be detected from the measured features. For each setting, eight time series of one minute duration were recorded at the flow rate $Q = 50\,\mathrm{m}^3/\mathrm{h}$. Two kinds of improper mounting were investigated: Off-axis mounting of the flowmeter and a DIN/ANSI mismatch in the diameter of the flowmeter pipe (ANSI, $d = 146.8\,\mathrm{mm}$) and the upstream and downstream pipe (DIN, $d = 159.3\,\mathrm{mm}$). The features D, S, G_r turned out to be the most efficient for this purpose. Figure 2 is as 3D scatter plot of the these features under all conditions. We evaluated this data under the assumption that, in practice, the kinematic

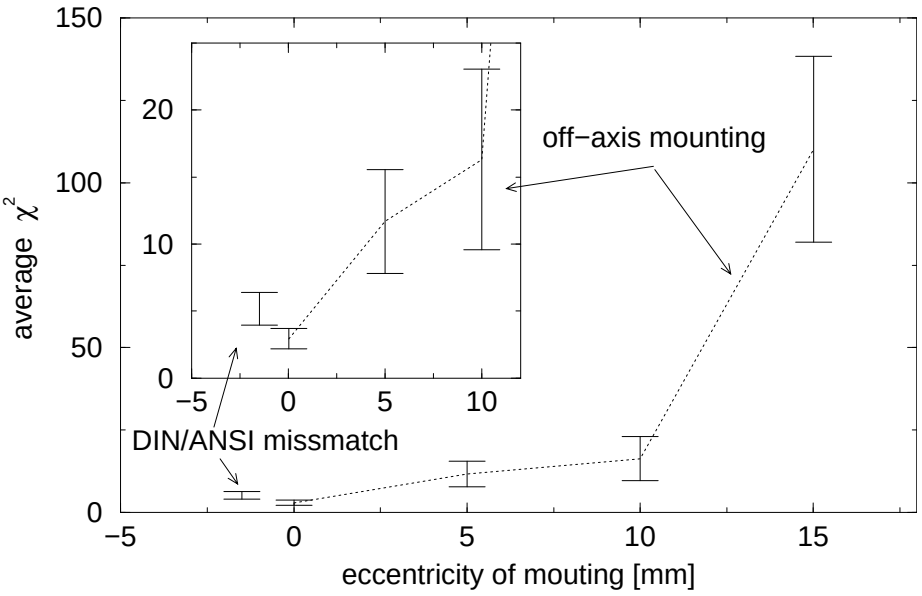

Figure 3: Average values of χ^2 derived from the sensor signal in order to detect inappropriate mounting. The data point for DIN/ANSI missmatch was shifted to the left. The inset is a blowup of the low-χ^2 region.

viscosity or, equivalently, the Reynolds number, are not known. Instead, a maximum likelihood estimate of the Reynolds number is used, assuming correct mounting. This leads to an estimate of the expectation values of D, S, and G_r corresponding to some flow rate in Fig. 1 or, respectively, to some point on the curve in Fig. 2.

With respect to these expectation values and the corresponding covariance matrix, χ^2 values were calculated for the differences $\mathbf{e} = (\Delta D, \Delta S, \Delta G_r)^T$ between the measured features and their expectation values, where χ^2 is given by

$$\chi^2 = \mathbf{e}^T \, \mathbf{C}^{-1} \, \mathbf{e} \tag{15}$$

and $\mathbf{C}$ is the covariance matrix. This quantity is used as a criterion to distinguish appropriate from inappropriate mounting. Situations with χ^2 value larger than some threshold (which depends on the confidence level) are identified as inappropriate mounting. In practical, on-line applications, a moving average over χ^2 might be a more appropriate criterion.

The average χ^2 values for the data collected for each experimental setting are shown in Fig. 3. The value increases drastically as the mounting conditions worsen. For symmetry reasons, one expects the average χ^2 values to be an even function in the eccentricity for off-axis mounting. Hence, the effect of off-axis mounting sets in quadratically with the eccentricity and is initially weak. For all cases of off-axis mounting the averages are significantly ($\alpha = 5\%$) increased

compared to ordinary mounting. Only for the DIN/ANSI mismatch the hypotheses of an average χ^2 equal to the value for ordinary mounting could not be rejected ($p = 0.07$). A repetition of the experiment for $Q = 100\,\mathrm{m}^3/\mathrm{h}$ gave similar results.

In order to assess the sensitivity of the method, we note that the shift in the vortex frequency due to inappropriate mounting and, as a result, the error in the flowmeter reading, is larger than 0.5% only for the 10mm and 15mm eccentricity cases. These can clearly be identified by an increase in χ^2. Thus, as a conservative estimate, irregularities that lead to more than 0.5% error in the output of the flowmeter can be detected.

5 Conclusion

A method for detecting inappropriate mounting for vortex flowmeters was demonstrated. The method is based on a general model of the sensor signal of the flowmeter. It is therefore expected to work also for other flowmeter geometries and to be able to detect several other kinds of faulty conditions, such as irregularities in the inlet or outlet piping, erosion of or depositions at the bluff body, or inhomogeneity of the fluid.

So far, the independence of the method from the material parameters of the fluid has not been verified experimentally. But the weak dependence of the scale-invariant features on the flow rate is a strong indication that the general theoretical considerations which lead to the predicted material independence are correct.

We acknowledge generous support by the German Bundesministerium für Bildung und Forschung (BMBF), grants 13N7954, 13N7955.

References

[1] V. Hans, G. Poppen, E. von Lavante, and S. Perpeet, "Vortex shedding flowmeters and ultrasound detection: Signal processing and influence of bluff body geometry," *Flow Meas. Instrum.*, vol. 9, pp. 79–82, June 1998.

[2] R. C. Mottram, "Vortex flowmeters – installation effects," *Flow Meas. Instrum.*, vol. 2, pp. 56–60, Jan 1991.

[3] T. T. Yeh and G. E. Mattingly, "Summary report of NIST's industry-government consortium research program on flowmeter installation effects: The 45 degree elbow," NISTR 1408, NIST (U.S.A.), Gaithersburg, MD, 1994.

[4] M. Henry, "Self-validating sensors," *Control Engineering Europe*, June 2001.

[5] J. E. Amadi-Echendy, H. Zhu, and E. H. Higham, "Analysis of signals from vortex flowmeters," *Flow Meas. Instrum.*, vol. 4, no. 4, pp. 225–231, 1993.

[6] S. Perovic, E. H. Higham, and P. J. Unsworth, "Fault detection and flow regime identification based on analysis of signal noise from electromagnetic flowmeters," in *Proceedings of the Institution of Mechanical Engineers, Part E (Journal of Process Mechanical Engineering)*, vol. 215, (London), pp. 283–294, Institution of Mechanical Engineers, 2001.

[7] C. Carlander and J. Delsing, "Installation effects on an ultrasonic flow meter with implications for self diagnostics," *Flow Meas. Instrum.*, vol. 11, pp. 109–122, June 2000.

[8] D. W. Clarke and T. Ghaoud, "Validation of vortex flowmeters," *Comp. Contr. Eng. J.*, vol. 13, pp. 237–241, Oct. 2002.

[9] D. W. Clarke and T. Ghaoud, "A dual phase-locked loop for vortex flow metering," *Flow Meas. Instrum.*, vol. 14, pp. 1–11, 2003.

[10] The diameter of the bluff body in typical flowmeters is within the same order of magnitude.

[11] C. Raman, M. Köhl, R. Onofrio, D. S. Durfee, C. E. Kuklewicz, Z. Hadzibabic, and W. Ketterle, "Evidence for a critical velocity in a Bose-Einstein condensed gas," *Phys. Rev. Lett.*, vol. 83, pp. 2502–2505, Aug. 1999.

[12] T. Winiecki, B. Jackson, J. McCann, and C. Adams, "Vortex shedding and drag in dilute Bose-Einstein condensates," *J. Physics B*, vol. 33, pp. 4069–4078, Oct 2000.

[13] K. R. Sreenivasan, P. J. Strykowski, and D. J. Olinger, "Hopf bifurcation, Landau equation, and vortex shedding behind circular cylinders," in *Proceedings of the forum on unsteady flow separation* (K. N. Ghia, ed.), vol. 52, pp. 1–13, New York: ASME, 1986.

[14] M. Provansal, C. Mathis, and L. Boyer, "Bénard-von Kármán instability: transient and forced regimes," *J. Fluid Mech.*, vol. 182, pp. 1–22, 1987.

[15] M. Schumm, E. Berger, and P. A. Monkewitz, "Self-excited oscillations in the wake of two-dimensional bluff bodies and their control," *J. Fluid Mech.*, vol. 271, pp. 17–53, 1994.

[16] P. Albarède and M. Provansal, "Quasi-periodic cylinder wakes and the Ginzburg-Landau model," *J. Fluid Mech.*, vol. 291, pp. 191–222, 1995.

[17] J. Dusek, P. L. Gal, and P. Fraunié, "A numerical and theoretical study of the first Hopf bifurcation in a cylinder wake.," *J. Fluid Mech.*, vol. 264, pp. 59–80, 1994.

[18] P. L. Gal, A. Nadim, and M. Thompson, "Hysteresis in the forced Stuart-Landau equation: Application to vortex shedding from an oscillating cylinder," *J. Fluids and Structures*, vol. 15, pp. 445–457, 2001.

[19] L. Arnold, *Random Dynamical Systems*. Berlin: Springer, 1998.

[20] J. Guckenheimer and P. Holmes, *Nonlinear Oscillations, Dynamical Systems and Bifurcations of Vector Fields*, vol. 42 of *Applied Mathematical Sciences*. New York: Springer, 1983.

[21] In fact, a faithful description requires corrections to the model. But these effects are small, and their quantitative characterization would be difficult.

[22] B. Boashash, "Estimating and interpreting the instantaneous frequeny of a signal.," *Proc. IEEE*, vol. 80, no. 4, pp. 520–568, 1992.

[23] H. Risken, *The Fokker-Planck Equation*, ch. 12. Berlin: Springer, 2nd ed., 1989.

[24] Produced by ABB Automation Products, Germany.